**The Cryosphere
Discussions**

Regional estimates of glacier mass change from MODIS-derived equilibrium line altitudes

J. M. Shea[1,2], B. Menounos[2], R. Dan Moore[1,3], and C. Tennant[2]

[1]Department of Geography, University of British Columbia, British Columbia, Canada
[2]Geography Program, University of Northern British Columbia, British Columbia, Canada
[3]Department of Forest Resource Management, University of British Columbia, British Columbia, Canada

Correspondence to: J. M. Shea (joseph.shea@geog.ubc.ca)

Title Page

Abstract	Introduction
Conclusions	References
Tables	Figures

|◀ | ▶|
◀ | ▶

Back | Close

Full Screen / Esc

Printer-friendly Version

Interactive Discussion

Abstract

We describe an automated method to extract regional snowline elevations and annual equilibrium line altitudes (ELAs) from daily MODIS imagery (MOD02QKM) on large glaciers and icefields in western North America. Regional MODIS-derived ELAs correlate significantly with observed net mass balance at six index glacier mass balance sites. Historical mass balance gradients were combined with MODIS-derived ELAs to estimate annual mass change at the Columbia, Lillooet, and Sittakanay icefields in British Columbia, Canada. Our approach yields estimates of mass change that are within 30 % of traditional geodetic approaches over decadal time-scales, and reveals continued mass loss of glaciers in western North America. Between 2000 and 2009, mean annual rates of surface elevation change for the Columbia, Lillooet, and Sittakanay icefields are estimated to be $-0.29 \pm 0.15\,\mathrm{m\,a^{-1}}$, $-0.57 \pm 0.10\,\mathrm{m\,a^{-1}}$, and $-0.90 \pm 0.09\,\mathrm{m\,a^{-1}}$, respectively. This study provides a complementary approach to the development of regional estimates of glacier mass change, which are critical for studies of glacier contributions to both streamflow and global sea-level rise.

1 Introduction

A substantial fraction of sea-level rise in the next century will originate from shrinking mountain glaciers and icecaps in response to anthropogenic climate change (Cazenave and Nerem, 2004; Raper and Braithwaite, 2006; Radić and Hock, 2011). Notable area and volume loss of glaciers (Larsen et al., 2007; Schiefer et al., 2007; Berthier et al., 2010; Bolch et al., 2010) and decreased late-summer flows for glacier fed rivers (Stahl and Moore, 2006; Moore et al., 2009) confirms that such responses already exist in western North America. On annual timescales, glacier mass change affects surface runoff in glacierized basins (Moore and Demuth, 2001), yet there are only a handful of mass change records in western North America.

MODIS-derived regional glacier mass change

J. M. Shea et al.

Long-term measurements of surface mass balance exist for fewer than 300 glaciers worldwide (Zemp et al., 2009). However, regional assessments of glacier mass change are required to quantify the non-steric fraction of sea level rise, assess changes in glacier contributions to streamflow, and manage water resources in mountain envi-
5   ronments. Currently, regional glacier mass change can be estimated from (a) ground-based measurements (Radić and Hock, 2010), (b) anomalies in regional gravity fields (Arendt et al., 2009; Jacob et al., 2012), (c) empirical models (Radić and Hock, 2011), (d) distributed mass balance models (Machguth et al., 2009), and (e) geodetic measurements (Schiefer et al., 2007; Tennant et al., 2012). However, these approaches
10   may be limited in terms of either spatial or temporal resolution, or both. Geodetic approaches, for example, are limited spatially by the availability of accurate digital elevation data, and temporally by the frequency of such data. Gravity-based methods are unable to resolve mass changes at the scale of individual watersheds or icefields. Distributed and empirical mass balance models rely on the sparse network of mass
15   balance observations for calibration and testing.

An alternative approach to estimate glacier mass change (Rabatel et al., 2005) exploits the relation between a glacier's annual net mass balance (B_n) and its transient snowline, which, at the end of the ablation season, closely mirrors the equilibrium line altitude (ELA). The ELA represents the elevation where accumulation is balanced by
20   ablation (Cogley et al., 2011). One advantage of using ELA to estimate B_n is that, with suitable space-borne sensors, it can be regularly measured across a region. Others have estimated glacier mass change from ELA observations with air photos (Østrem, 1973) or optical imagery (Rabatel et al., 2005), but the 14-day repeat cycle of Landsat, for example, limits its application in mountain environments with pervasive cloud cover.
25   The MODIS (Moderate Resolution Imaging Spectroradiometer) sensor provides an opportunity to monitor the transient snowline on large mid-latitude glaciers across the globe on a daily basis. The MOD10 snow cover product (Hall et al., 2002), based on Normalized Difference Snow Index (NDSI) thresholds, has been used to validate hydrological models (Parajka and Blöschl, 2008) and to map snow cover in large watersheds

(Déry and Brown, 2007). Unfortunately, it is not possible to map glacier ELAs from the MOD10 product, given its 500 m resolution and poor discrimination between snow and ice (Hall and Riggs, 2007). The MOD02QKM product contains calibrated and geolocated radiances in the red (0.620–0.670 µm) and near infrared (0.841–0.876 µm) bands with spatial resolutions of 250 m at nadir. Others have used these bands to calculate sub-pixel fractional snow cover and monitor snowline evolution (Lopez et al., 2008; Sirguey et al., 2009), and a recent study developed estimates of mass change from MODIS-derived surface albedos (Dumont et al., 2012).

In this study, we employ the 250 m visible and near-infrared bands of MODIS to estimate transient snowline elevations and annual ELA for glaciers and icefields in western North America. Relations between regional MODIS-derived ELAs and ground-based observations of glacier mass balance at seven index glacier sites are examined, and correlations and trends in regional ELA are identified. We extend our approach to estimate the mass change of three large icefields using historical mass balance gradients, and compare these results to geodetic estimates of mass change. Basin-scale estimates of glacier mass change are useful for diagnosing glacier contributions to streamflow and sea-level rise, and the approach developed here complements other estimates of glacier mass change.

2 Data and methods

2.1 Site selection

Our analyses focus on index glacier mass balance sites near large icefields in western North America where either ground observations of surface mass balance or geodetic estimates of glacier mass change are available. Between 2000 and 2009, specific surface mass balance data (M. Zemp, personal communication, 2011) are available at eight index glacier mass balance sites (Fig. 1). We also selected three large icefields (Columbia, Lillooet, and Sittakanay) where both (a) historical mass balance data

by elevation band and (b) geodetic estimates of glacier mass change are available. Peyto Glacier is a long-term mass balance monitoring site, located approximately 75 km south-east of the Columbia Icefield (Fig. 2), and mass balance data are available from 1965–2005 (Mokievsky-Zubok et al., 1985; Dyurgerov, 2002). Bridge Glacier is a tributary of the Lillooet Icefield (Fig. 3), and mass balance data by elevation band are available from 1977–1985 (Mokievsky-Zubok et al., 1985; Dyurgerov, 2002). Mass balance data for the Andrei Glacier from 1977–1985 were obtained from Mokievsky-Zubok et al. (1985) and Dyurgerov (2002), with additional mass balance data for 1989–1991 extracted from BC Hydro reports (Mokievsky-Zubok, 1990, 1991, 1992). Andrei Glacier lies approximately 100 km south east of the Sittakanay Icefield (Fig. 1).

2.2 MOD02QKM classification and ELA

MOD02QKM and MOD10L2 scenes covering western North America were obtained for the end of the ablation season (15 August–15 October) between 2000 and 2009 (NASA, 2012b; Hall et al., 2012). MOD02QKM and MOD10L2 imagery were first projected to BC Albers using the the HEG toolkit. The MOD10L2 product was then resampled to 250 m resolution, and we extracted the MOD10L2 cloud mask and applied it to the MOD02QKM imagery. The resulting scenes were clipped using publicly available digital outlines of the glaciers (Armstrong et al., 2012) in each region. At each site and day, we then used an unsupervised k-means cluster analysis of the visible and near-infrared bands to classify all glacierized and cloud-free pixels as either snow or ice. To avoid sampling errors due to excessively cloudy conditions or fresh snowfall events, we only analysed scenes with less than 50 % cloud cover and greater than 5 % ice cover, as defined by the MOD10L2 product.

2.3 Estimation of ELA

To define the seasonal ELA for a given glacierized region, we constructed time series of snowline elevation. Localized enhancements of accumulation (e.g. by wind

MODIS-derived regional glacier mass change

J. M. Shea et al.

redistribution) or ablation (e.g. south-facing slopes) will result in variations in snow-line elevation across the surface of a glacier or icefield on any given day. Thus, we use digital elevation models (DEMs) from GTED and SRTM (Gesch et al., 2002; Farr et al., 2007), resampled to 250 m resolution, to calculate mean, range, and quantiles of elevation for the snow and ice classes for each scene and region.

At most index glacier mass balance sites, the 20th percentile of elevation of snow-covered pixels ($Z_{S(20)}$) yielded the best correlation to observed surface mass balance, and so we select this metric to represent the elevation of the local transient snow-line. The $Z_{S(20)}$ metric appears insensitive to geospatial or glacier delineation errors, which may cause bare rock pixels at higher elevations to be included and classified as ice. Locally weighted least squares (lowess) regressions, with points weighted by the proportion of cloud-free pixels, were used to define seasonal time series of snowline elevations for each site (e.g. Fig. 4). The maximum value of each lowess curve was then taken as the end-of-season snowline, or annual ELA.

2.4 Regional glacier mass change

We extend the approach of Rabatel et al. (2005) to estimate annual net mass balance at 100 m elevation bands (b_n) using a piecewise linear spline (Fountain and Vecchia, 1999) with separate mass balance gradients above and below the MODIS-derived ELA:

$$b_{n(j)} = \begin{cases} b_1 (b_0 - Z_j), \, Z_j \leq b_0 \\ b_2 (Z_j - b_0), \, Z_j > b_0 \end{cases} \tag{1}$$

where b_0 is the MODIS-derived ELA (m), b_1 and b_2 are mass balance gradients (mm w.e. m^{-1}), and Z_j is the midpoint of elevation band j (m).

To evaluate this approach, we compare MODIS- and geodetically-derived estimates of mass change at the Columbia, Lillooet and Sittakanay icefields. Using SPOT and SRTM DEMs (Table 1), we calculate geodetic balance with an approach described

elsewhere (Schiefer et al., 2007; Tennant et al., 2012). Values for b_1 and b_2 at each icefield were obtained by setting b_0 as a free parameter, and fitting Eq. (1) to annual net mass balance observations at Peyto, Bridge, and Andrei glaciers (Fig. 5). Average fitted values for b_1 and b_2 range from 5.17 to 7.25 mm m^{-1} and 2.15 to 4.07 mm m^{-1}, respectively.

Hypsometric data derived from the GLIMS glacier boundaries and the SRTM DEMs were then used with Eq. (1) to estimate annual B_n. Errors in MODIS-derived estimates of volume change were estimated from the standard error in the weighted $Z_{S(20)}$ lowess curves and an assumed error in mass balance gradients of 10 %. Uncertainty in $Z_{S(20)}$ is primarily related to the frequency of cloud-free scenes.

3   Results

3.1   Glacier surface classification

At all sites examined, glacier surface types extracted from the MOD02QKM cluster analyses compare favourably with contemporaneous Landsat false-colour composites (NASA, 2012a). Additionally, our MOD02QKM clusters better discriminate between snow and ice surfaces than the MOD10 binary snow cover product (Figs. 2 and 3). As the presence/absence of snow in the MOD10 product is based on a threshold NDSI value, calculated from MODIS bands 4 and 6 (Hall et al., 2002), further investigations into the specific threshold over glacierized surfaces is recommended.

3.2   MODIS-derived ELAs and index glacier mass balance

At most index glacier mass balance sites in western North America, MODIS-derived regional ELAs are correlated with observed net mass balances (Fig. 6). Simple linear regressions between regional ELA and observed B_n are significant at $\alpha = 0.05$ for both Peyto and Wolverine, and significant at $\alpha = 0.10$ for Gulkana, Lemon Creek, and Taku.

No significant relations exist between MODIS-derived ELAs and B_n at Place or Emmons. Reasons for this may include the small sample size at Emmons Glacier ($n = 4$) or the lack of representativenes of Place Glacier within its defined region.

Over the period 2000–2011, MODIS-derived regional ELAs increased at the Peyto and Gulkana index mass balance sites, both continental glaciers. The annual change in regional snowline elevation at Gulkana Glacier and Peyto Glacier, respectively, were $+16.8\,\text{m}\,\text{a}^{-1}$ ($p = 0.04$), and $+2.9\,\text{m}\,\text{a}^{-1}$ ($p = 0.09$). No significant trends in regional ELA exist were found at other index glacier sites.

Simple correlations calculated between regional ELA anomalies (Table 3) suggest that glaciers across western North America display complex relations. Regional ELA anomalies derived for the Peyto Glacier region, for example, are significantly correlated ($r = 0.75$) with those obtained for the Columbia Icefield, but regional ELAs at Place Glacier are not significantly correlated with those observed at the Lillooet Icefield, which is located only 75 km to the northeast (Fig. 1). Regional ELA anomalies observed at the South Cascade site are significantly correlated with a number of locations in the Pacific Northwest, including Peyto Glacier ($r = 0.50$), Emmons Glacier ($r = 0.61$), Lillooet Icefield ($r = 0.72$) and Place Glacier ($r = 0.84$). Weak negative correlations between regional ELAs observed at Alaskan (Wolverine and Gulkana) and southern sites (Emmons, Place, Lillooet) support previously documented reversals in mass balance signals in response to large-scale atmospheric circulation patterns (Bitz and Battisti, 1999; McCabe et al., 2000).

3.3 MODIS-derived estimates of glacier mass change

MODIS-derived estimates of glacier mass change reasonably agree with those obtained using a geodetic approach (Table 2), and our results are consistent with those obtained by Schiefer et al. (2007), hereafter S07. At all sites, surface thinning is observed between 2000 and 2009. Compared to rates observed for 1985–1999, our results suggest a decreased rate of mass loss at the Columbia Icefield, and no real change in the rate of mass loss at the Lillooet or Sittakanay icefields. For the Lillooet

Icefield, geodetic- and MODIS-derived rates of surface elevation change calculated between 2000 and 2009 are −0.67 and −0.57 m a^{-1}, respectively, compared to a rate of −0.6 m a^{-1} between 1970 and 1988 (S07). Geodetic- and MODIS-derived rates of surface elevation change calculated for the Columbia Icefield (−0.30 and −0.29 m a^{-1}, respectively) are half those observed between 1985 and 1999 (−0.64 m a^{-1}, S07). Previously reported rates of surface elevation change at the Andrei Icefield ranged between −0.5 (1965–1982) and −1.1 (1985–1999) m a^{-1} (S07). Both our geodetic and MODIS-derived estimates of mass change between 2000 and 2007 (−0.68 and −0.90 m a^{-1}, respectively) suggest continued high rates of mass loss in this region.

4 Discussion

This research demonstrates a technique for constructing time series of transient snow-line elevations and equilibrium line altitudes on large glaciers and icefields using moderate resolution optical imagery. Significant relations exist between MODIS-derived regional ELAs and glacier mass balances observed at index glacier mass balance monitoring sites. When the approach was applied to three unmonitored icefields, using mass balance gradients calculated from observations that were temporally and/or spatially distant from the icefields, estimates of mass change were (a) within 30 % of geodetically derived estimates and (b) consistent with previous studies.

Possible sources of error in MODIS-derived estimates of glacier mass change include (1) improperly specified mass balance gradients, (2) errors in MODIS-derived ELAs, and (3) differences in the dates of geodetic image acquisition and our calculation of end-of-season glacier mass change. Mass balance gradients calculated for Peyto Glacier ($n = 44$) show standard deviations of 1.33 and 1.97 mm m^{-1} below and above the ELA, respectively, and no temporal trends. However, it is possible that shorter mass balance records, or those that do not correspond with the dates of ELA observation (e.g. at Bridge and Andrei glaciers) are unsuitable for estimation of glacier mass change. Additionally, the extrapolation of mass balance gradients below the elevation

range of the observations may introduce additional errors (e.g. at Sittakanay Icefield, Fig. 5). Future research aims to develop regionally distributed mass balance fields that can be used to estimate mass balance gradients.

Equilibrium line altitudes derived from the classification of MOD02QKM imagery will be sensitive to the availability of cloud-free imagery, and may not reflect the mass balance gradients calculated for index glaciers. The use of lowess smoothers provides a conservative estimate of the maximum value of $Z_{s(20)}$. However, this value will not necessarily correspond with the ELA observed at the index glacier due to the regional variability of snowline elevation. Finally, there may be a small source of error introduced by differences in the dates of geodetic image acquisition and our assumed end of ablation season calculations of mass change. SRTM data were collected in February 2000, and our assumption that this represents the end-of-summer surface elevation in 1999 may introduce a seasonal snow accumulation signal. We further assume that SPOT data collected in late August 2009 (Columbia, Lillooet) represents the surface elevation at the end of 2009, while SPOT data collected in early July 2008 (Sittakanay) represent the surface elevation at the end of 2007. Significant amounts of glacier ice melt will occur in July when glacier ice is exposed and solar radiation and air temperatures remain high.

The advantages of using MODIS imagery to derive changes in glacier mass over other approaches include daily frequency, global coverage, and low input data requirements. Our results are primarily limited by the need for appropriate mass balance gradients, by the size of the glacierized area being analyzed, and by the availability of cloud-free scenes. The approach developed in this study is not applicable for tidewater glaciers or debris-covered glaciers, but it could be employed in regions where observations or modelled estimates of glacier mass balance gradients are available. Our approach complements other methods for estimating regional glacier mass change and glacier contributions to streamflow and sea-level rise. We recommend further comparisons between the MODIS-derived ELA method developed here and the MODIS-retrieved albedo approach (Dumont et al., 2012). Where suitable test data exist, future

research should also determine if cluster analysis methods are sufficient for extracting three glacier surface classes (snow, firn, and ice). Finally, glacier snow cover maps developed in this study can be used to calibrate and test distributed glacier mass balance and hydrologic models.

5   Conclusions

Cluster analyses of MOD02QKM visible and near-infrared imagery were used to generate daily ablation season snow and ice coverages over large glaciers and icefields, with marked improvements over the MOD10 snow product. Significant relations exist between ground-based mass balance observations and regional MODIS-derived ELAs. When applied to individual icefields, estimates of total mass change generated from MODIS-derived ELAs and geodetic approaches agree to within 30 % on decadal timescales. Our results are consistent with the rates of mass change observed in previous studies, and we find continued overall net mass loss at three large icefields in western North America. MODIS-derived glacier mass change estimates can effectively complement other approaches to gauge the mass change of large mountain glaciers and icefields, which are expected to be the largest contributors to sea-level rise over the next century.

Title Page

Abstract | Introduction

Conclusions | References

Tables | Figures

|◄ | ►|

◄ | ►

Back | Close

Full Screen / Esc

Printer-friendly Version

Interactive Discussion

References

Arendt, A. A., Luthcke, S. B., and Hock, R.: Glacier changes in Alaska: can mass-balance models explain GRACE mascon trends?, Ann. Glaciol., 50, 148–154, doi:10.3189/172756409787769753, 2009. 3759

Armstrong, R., Raup, B., Khalsa, S., Barry, R., Kargel, J., Helm, C., and Kieffer, H.: GLIMS glacier database, Digital Media, National Snow and Ice Data Center, Boulder, Colorado, USA, 2012. 3761

Berthier, E., Schiefer, E., Clarke, G. K. C., Menounos, B., and Rémy, F.: Contribution of Alaskan glaciers to sea-level rise derived from satellite imagery, Nat. Geosci., 3, 92–95, doi:10.1038/ngeo737, 2010. 3758

Bitz, C. M. and Battisti, D. S.: Interannual to decadal variability in climate and the glacier mass balance in Washington, Western Canada, and Alaska, J. Climate, 12, 3181–3196, 1999. 3764

Bolch, T., Menounos, B., and Wheate, R.: Landsat-based inventory of glaciers in Western Canada, 1985–2005, Remote Sens. Environ., 114, 127–137, 2010. 3758

Cazenave, A. and Nerem, R. S.: Present-day sea level change: observations and causes, Rev. Geophys., 42, RG3001, doi:10.1029/2003RG000139, 2004. 3758

Cogley, J., Hock, R., Rasmussen, L., Arendt, A., Bauder, A., Braithwaite, R., Jansson, P., Kaser, G., Möller, M., Nicholson, L., and Zemp, M.: Glossary of glacier mass balance and related terms, IHP-VII Technical Documents in Hydrology No. 86, IACS Contribution No. 2, 126 pp., 2011. 3759

Déry, S. J. and Brown, R. D.: Recent Northern Hemisphere snow cover extent trends and implications for the snow-albedo feedback, Geophys. Res. Lett., 34, L22504, doi:10.1029/2007GL031474, 2007. 3760

Dumont, M., Gardelle, J., Sirguey, P., Guillot, A., Six, D., Rabatel, A., and Arnaud, Y.: Linking glacier annual mass balance and glacier albedo retrieved from MODIS data, The Cryosphere Discuss., 6, 2363–2398, doi:10.5194/tcd-6-2363-2012, 2012. 3760, 3766

Dyurgerov, M.: Glacier mass balance and regime: data of measurements and analysis, Institute of Arctic and Alpine Research, Occasional Paper 55, University of Colorado, 2002. 3761

Title Page

Abstract | Introduction

Conclusions | References

Tables | Figures

◄◄ | ►►

◄ | ►

Back | Close

Full Screen / Esc

Printer-friendly Version

Interactive Discussion

Farr, T. G., Rosen, P. A., Caro, E., Crippen, R., Duren, R., Hensley, S., Kobrick, M., Paller, M., Rodriguez, E., Roth, L., Seal, D., Shaffer, S., Shimada, J., Umland, J., Werner, M., Oskin, M., Burbank, D., and Alsdorf, D.: The shuttle radar topography mission, Rev. Geophys., 45, RG2004, doi:10.1029/2005RG000183, 2007. 3762

Fountain, A. G. and Vecchia, A.: How many stakes are required to measure the mass balance of a glacier?, Geogr. Ann. A, 81, 563–573, 1999. 3762

Gesch, D., Oimoen, M., Greenlee, S., Nelson, C., Steuck, M., and Tyler, D.: The national elevation dataset, Photogramm. Eng. Rem. S., 68, 5–11, 2002. 3762

Hall, D., Riggs, G., Salomonson, V., DiGirolamo, N., and Bayr, K.: MODIS snow-cover products, Remote Sens. Environ., 83, 181–194, 2002. 3759, 3763

Hall, D., Riggs, G., and Salomonson, V.: MODIS/Terra Snow Cover 5-min L2 Swath 500 m V005, 2000–2009, Digital Media, National Snow and Ice Data Center, Boulder, CO, 2012. 3761

Hall, D. K. and Riggs, G. A.: Accuracy assessment of the MODIS snow products, Hydrol. Process., 21, 1534–1547, doi:10.1002/hyp.6715, 2007. 3760

Jacob, T., Wahr, J., Pfeffer, W., and Swenson, S.: Recent contributions of glaciers and ice caps to sea level rise, Nature, 482, 514–518, doi:10.1038/nature10847, 2012. 3759

Larsen, C. F., Motyka, R. J., Arendt, A. A., Echelmeyer, K. A., and Geissler, P. E.: Glacier changes in southeast Alaska and northwest British Columbia and contribution to sea level rise, J. Geophys. Res.-Earth, 112, F01007, doi:10.1029/2006JF000586, 2007. 3758

Lopez, P., Sirguey, P., Arnaud, Y., Pouyaud, B., and Chevallier, P.: Snow cover monitoring in the Northern Patagonia Icefield using MODIS satellite images (2000–2006), Global Planet. Change, 61, 103–116, doi:10.1016/j.gloplacha.2007.07.005, 2008. 3760

Machguth, H., Paul, F., Kotlarski, S., and Hoelzle, M.: Calculating distributed glacier mass balance for the Swiss Alps from regional climate model output: a methodical description and interpretation of the results, J. Geophys. Res.-Atmos., 114, D19106, doi:10.1029/2009JD011775, 2009. 3759

McCabe, G. J., Fountain, A. G., and Dyurgerov, M.: Variability in winter mass balance of Northern Hemisphere glaciers and relations with atmospheric circulation, Arct. Antarct. Alp. Res., 32, 64–72, 2000. 3764

Mokievsky-Zubok, O.: Glaciological studies in Iskut River Basin, 1989, Internal Report, B. C. Hydro, 1990. 3761

Title Page

Abstract | Introduction

Conclusions | References

Tables | Figures

|◄ | ►|

◄ | ►

Back | Close

Full Screen / Esc

Printer-friendly Version

Interactive Discussion

Mokievsky-Zubok, O.: Glaciological studies in Iskut River Basin, 1990, Internal Report, B. C. Hydro, 1991. 3761

Mokievsky-Zubok, O.: Glaciological studies in Iskut River Basin, 1991, Internal Report, B. C. Hydro, 1992. 3761

5 Mokievsky-Zubok, O., Ommanney, O. S. J., and Power, J.: NHRI Glacier Mass Balance 1964–1984 (Cordillera and Arctic), National Hydrology Research Institute, Environment Canada, 59 pp., 1985. 3761

Moore, R. D. and Demuth, M. N.: Mass balance and streamflow variability at Place Glacier, Canada, in relation to recent climate fluctuations, Hydrol. Process., 15, 3473–3486, doi:10.1002/hyp.1030, 2001. 3758

10 Moore, R. D., Fleming, S. W., Menounos, B., Wheate, R., Fountain, A., Stahl, K., Holm, K., and Jakob, M.: Glacier change in Western North America: influences on hydrology, geomorphic hazards and water quality, Hydrol. Process., 23, 42–61, doi:10.1002/hyp.7162, 2009. 3758

NASA: Landsat TM and ETM+, 2000–2009, Digital Media, USGS, available at: http://glovis.usgs.gov/ (last access: July 2012), 2012a. 3763

15 NASA: MODIS/Terra Calibrated Radiances 5-Min L1B Swath 250 m, 2000–2009, Digital Media, Level 1 and Atmsophere Archive and Distribution System, available at: http://ladsweb.nascom.nasa.gov/ (last access: July 2012), 2012b. 3761

Østrem, G.: The transient snowline and glacier mass balance in Southern British Columbia and Alberta, Canada, Geogr. Ann. A, 55, 93–106, 1973. 3759

20 Parajka, J. and Blöschl, G.: The value of MODIS snow cover data in validating and calibrating conceptual hydrologic models, J. Hydrol., 358, 240–258, 2008. 3759

Rabatel, A., Dedieu, J.-P., and Vincent, C.: Using remote-sensing data to determine equilibrium-line altitude and mass-balance time series: validation on three French glaciers, 1994–2002, J. Glaciol,, 51, 539–546, doi:10.3189/172756505781829106, 2005. 3759, 3762

25 Radić, V. and Hock, R.: Regional and global volumes of glaciers derived from statistical upscaling of glacier inventory data, J. Geophys. Res.-Earth, 115, F01010, doi:10.1029/2009JF001373, 2010. 3759

Radić, V. and Hock, R.: Regionally differentiated contribution of mountain glaciers and ice caps to future sea-level rise, Nat. Geosci., 4, 91–94, doi:10.1038/ngeo1052, 2011. 3758, 3759

30 Raper, S. C. B. and Braithwaite, R. J.: Low sea level rise projections from mountain glaciers and icecaps under global warming, Nature, 439, 311–313, doi:10.1038/nature04448, 2006. 3758

MODIS-derived regional glacier mass change

J. M. Shea et al.

Title Page

Abstract	Introduction
Conclusions	References
Tables	Figures

|◄ | ►|

◄ | ►

Back | Close

Full Screen / Esc

Printer-friendly Version

Interactive Discussion

Schiefer, E., Menounos, B., and Wheate, R.: Recent volume loss of British Columbian Glaciers, Canada, Geophys. Res. Lett., 34, L16503, doi:10.1029/2007GL030780, 2007. 3758, 3759, 3763, 3764

Sirguey, P., Mathieu, R., and Arnaud, Y.: Subpixel monitoring of the seasonal snow cover with MODIS at 250 m spatial resolution in the Southern Alps of New Zealand: methodology and accuracy assessment, Remote Sens. Environ., 113, 160–181, 2009. 3760

Stahl, K. and Moore, R. D.: Influence of watershed glacier coverage on summer streamflow in British Columbia, Canada, Water Resour. Res., 42, W06201, doi:10.1029/2006WR005022, 2006. 3758

Tennant, C., Menounos, B., Ainslie, B., Shea, J., and Jackson, P.: Comparison of modeled and geodetically-derived glacier mass balance for Tiedemann and Klinaklini glaciers, Southern Coast Mountains, British Columbia, Canada, Global Planet. Change, 82, 74–85, doi:10.1016/j.gloplacha.2011.11.004, 2012. 3759, 3763, 3773

Zemp, M., Hoelzle, M., and Haeberli, W.: Six decades of glacier mass-balance observations: a review of the worldwide monitoring network, Ann. Glaciol., 50, 101–111, doi:10.3189/172756409787769591, 2009. 3759

Title Page

Abstract | Introduction

Conclusions | References

Tables | Figures

|◄ | ►|

◄ | ►

Back | Close

Full Screen / Esc

Printer-friendly Version

Interactive Discussion

Table 1. Imagery used in geodetic mass change calculations.

Site	Imagery	Date of Acquisition
Columbia	SRTM	Feb 2000
	SPOT-5	20 Aug 2009
	SPOT-5	30 Aug 2009
Lillooet	SRTM	Feb 2000
	SPOT-5	29 Aug 2009
	SPOT-5	20 Aug 2009
Sittakanay	SRTM	Feb 2000
	SPOT-5	02 Jul 2008

Table 2. Geodetic and MODIS-derived estimates of glacier mass change (Gt), for Columbia and Lillooet icefields. Percent difference (%) is calculated relative to the geodetic estimate of mass change.

Site	Area (km^2)	Period	Geodetic[a]	MODIS	Difference (%)
Columbia	216	2000–2009	-0.65 ± 0.10	-0.63 ± 0.33	-3.1
Lillooet	490	2000–2009	-3.31 ± 0.57	-2.81 ± 0.50	-15.1
Sittakanay	416	2000–2007[b]	-2.26 ± 0.11	-3.00 ± 0.26	$+32.7$

[a] Error term derived by standard propagation of errors (Tennant et al., 2012)
[b] Geodetic balance calculated from February 2000 to 2 July 2008

Title Page

Abstract | Introduction

Conclusions | References

Tables | Figures

|◄ | ►|

◄ | ►

Back | Close

Full Screen / Esc

Printer-friendly Version

Interactive Discussion

Table 3. Regional ELA anomaly correlation matrix. Correlations significant at $\alpha = 0.10$ and $\alpha = 0.05$ are indicated by one and two asterixes, respectively.

	Columbia	Emmons	Gulkana	Juneau	Lillooet	Peyto	Place	Sittakanay	S. Cascade	Wolverine
Columbia	1.00	0.62**	0.24	0.51*	0.52*	0.75**	0.02	0.16	0.46	0.11
Emmons	0.62**	1.00	−0.32	−0.01	0.59**	0.27	0.39	−0.25	0.61**	−0.22
Gulkana	0.24	−0.32	1.00	0.35	0.26	0.41	−0.22	0.20	0.08	0.23
Juneau	0.51*	−0.01	0.35	1.00	0.37	0.82**	0.09	0.73**	0.24	0.45
Lillooet	0.52*	0.59**	0.26	0.37	1.00	0.48	0.48	0.24	0.72**	−0.17
Peyto	0.75**	0.27	0.41	0.82**	0.48	1.00	0.21	0.49	0.50*	0.17
Place	0.02	0.39	−0.22	0.09	0.48	0.21	1.00	0.15	0.84**	0.06
Sittakanay	0.16	−0.25	0.20	0.73**	0.24	0.49	0.15	1.00	0.06	0.27
S. Cascade	0.46	0.61**	0.08	0.24	0.72**	0.50*	0.84**	0.06	1.00	0.02
Wolverine	0.11	−0.22	0.23	0.45	−0.17	0.17	0.06	0.27	0.02	1.00

Columbia Icefield

Lillooet Icefield

Sittakanay Icefield

1. Andrei Glacier
2. Columbia Icefield
3. Emmons Glacier
4. Gulkana Glacier
5. Lemon Creek Glacier
6. Lillooet Icefield
7. Peyto Glacier
8. Place Glacier
9. Sittakanay Icefield
10. South Cascade Glacier
11. Taku Glacier
12. Wolverine Glacier
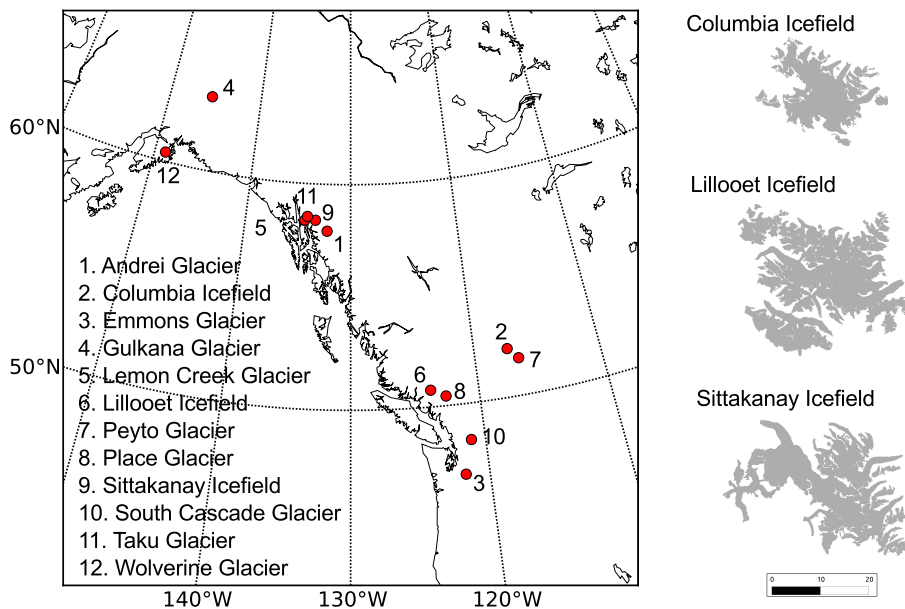
Fig. 1. Study area, with locations of index glaciers and geodetic mass balance sites. Columbia, Lillooet, Sittakany icefields are all shown to scale.
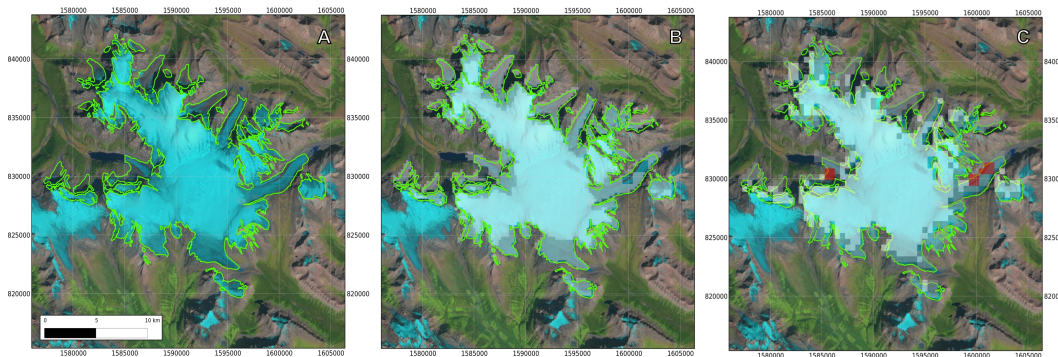
Fig. 2. (A) Landsat 5 scene of Columbia Icefield, 29 August 2009, with **(B)** corresponding MOD02 snow (white) and ice (gray) clusters, and **(C)** MOD10 snow cover product. Cloud-obscured pixels in **(C)** are shown in red. Imagery is shown in BC Albers projection.
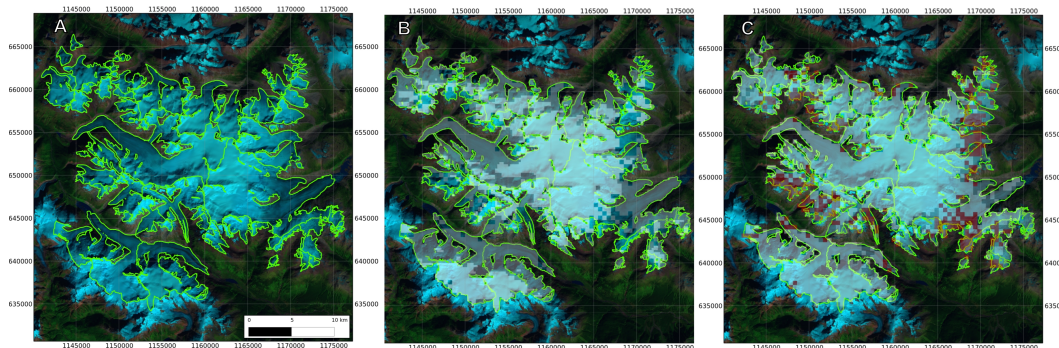
Fig. 3. (A) Landsat 5 scene of Lillooet Icefield, 5 September 2001, with **(B)** corresponding MOD02 snow (white) and ice (gray) clusters, and (C) MOD10 snow cover product. Cloud-obscured pixels in **(C)** are shown in red. Imagery is shown in BC Albers projection.
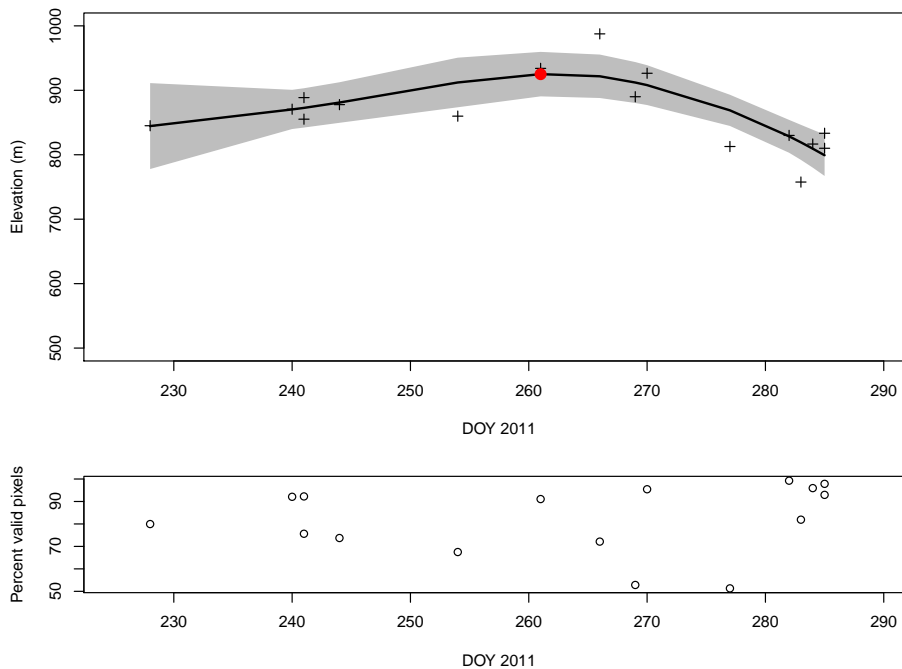
Fig. 4. Top panel: observations (crosses) of $Z_{S(20)}$ by day of year (DOY) for the Wolverine Glacier region, 2011 ablation season. The lowess curve (black) with standard errors (grey) is weighted by the percentage of cloud-free pixels (bottom panel) in each scene. The maximum value on the lowess curve (red) is assumed to represent the annual ELA.
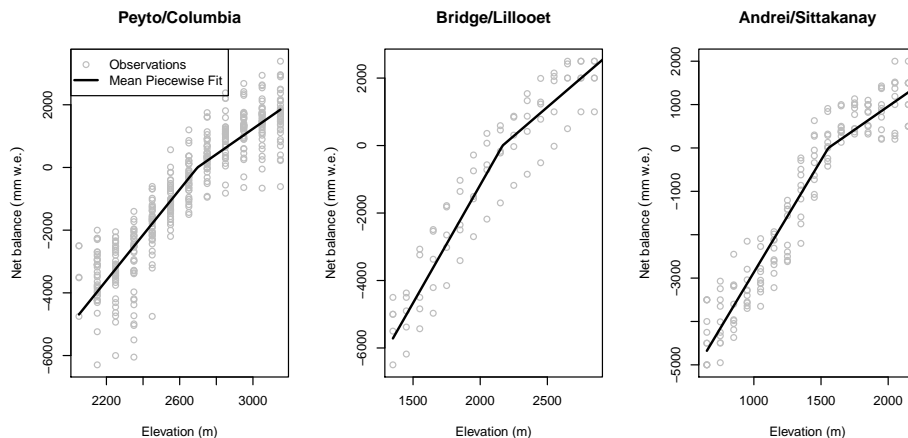
Fig. 5. Observed net mass balance by elevation band for Peyto (Columbia), Bridge (Lillooet), and Andrei (Sittakanay) glaciers and icefields. Solid black lines give mean fitted mass balance gradients.
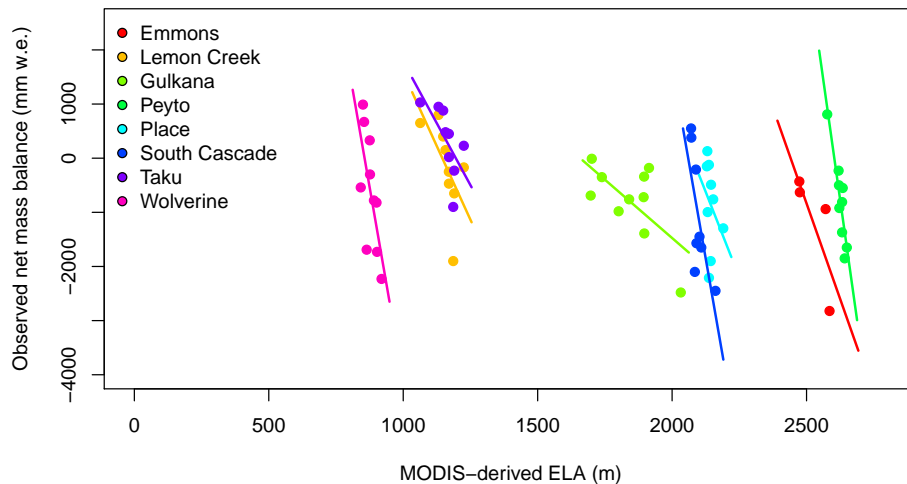
Fig. 6. Observed net mass balance at eight index sites and MODIS-derived regional ELA, 2000–2009.